Water Research, Volume 107, 1ssue December, 2016, pp. 102-112
DOI:10.1016/j.watres.2016.10.060

Accepted Manuscript

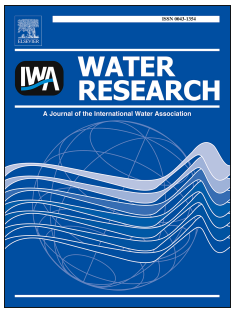

The effect of high hydraulic loading rate on the removal efficiency of a quadruple media filter for tertiary wastewater treatment

Philani Ncube, Marc Pidou, Tom Stephenson, Bruce Jefferson, Peter Jarvis

PII: S0043-1354(16)30813-2

DOI: 10.1016/j.watres.2016.10.060

Reference: WR 12458

To appear in: *Water Research*

Received Date: 30 June 2016

Revised Date: 23 September 2016

Accepted Date: 22 October 2016

Please cite this article as: Ncube, P., Pidou, M., Stephenson, T., Jefferson, B., Jarvis, P., The effect of high hydraulic loading rate on the removal efficiency of a quadruple media filter for tertiary wastewater treatment, *Water Research* (2016), doi: 10.1016/j.watres.2016.10.060.

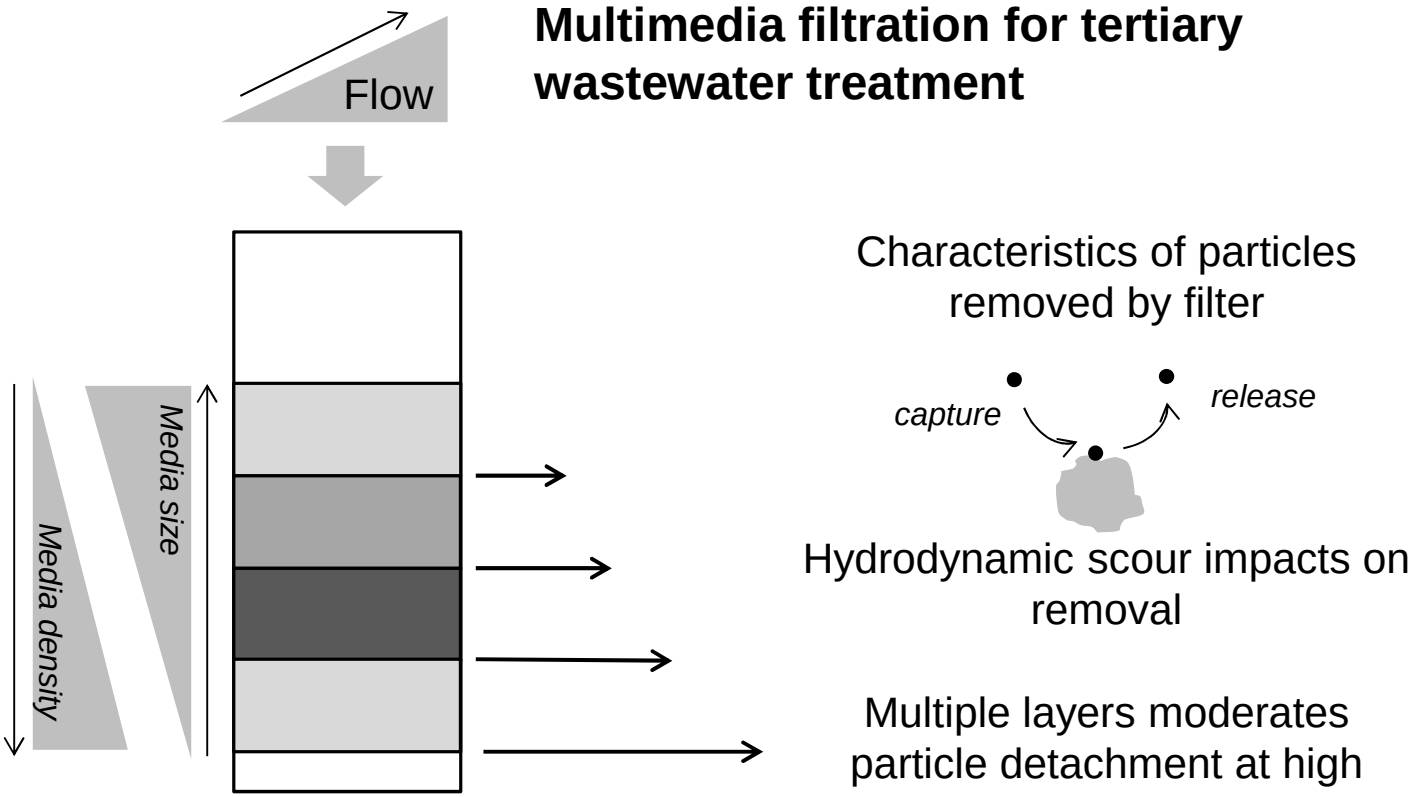
Flow
Multimedia filtration for tertiary wastewater treatment
Media size
Media density
Characteristics of particles removed by filter
capture
release
Hydrodynamic scour impacts on removal
Multiple layers moderates particle detachment at high flows

The effect of high hydraulic loading rate on the removal efficiency of a quadruple media filter for tertiary wastewater treatment

*Philani Ncube, Marc Pidou, Tom Stephenson, Bruce Jefferson, Peter Jarvis**

[a]Cranfield Water Science Institute, Cranfield University, College Road, Cranfield, Bedfordshire, MK43 0TE UK.

[*]Corresponding author: p.jarvis@cranfield.ac.uk, 00 44 1234 750111 ext 3374

Abstract

It is well known that filtration removal efficiency falls with an increase in flow rate; however, there is limited supporting experimental data on how removal efficiency changes for filters with multiple layers of media and for wastewater filtration, a practice that is becoming more common. Furthermore, information is not available on the characteristics of particles that are removed at different flow rates. Here, a quadruple media filter was operated at hydraulic loading rates (HLRs) between 5 and 60 mh^{-1} with subsequent measurement of total suspended solids, turbidity and particle size distribution (PSD). Samples were collected from the filter influent, effluent and also from between media layers. Pressure changes across the filter layers were also measured. The solids removal efficiency of the filter varied inversely with the increase in filtration rate. However, the multiple media layers reduced the negative impact of increased HLR in comparison to a single media filter. High filtration rates were shown to transport solids, such that particle retention and headloss development was distributed across the entire depth of the multi-media filter. There was also a progressive decrease in the suspension particle size leaving each of the filter layers. The particle

hydrodynamic force simulation was consistent with the changes in measured PSD through the filter layers.

Introduction

Granular media filtration is one of the oldest forms of treatment technology used in the production of potable water and is still widely used due to its reliability and low cost (Burton et al., 2003; Han et at., 2009; Kim et al., 2012). However, the filtration of wastewater secondary effluent is a relatively recent practice in situations that demand high water quality. This includes tertiary treatment of wastewater for water reuse in water stressed areas (Bloetscher et al., 2014; Christou et al., 2014; Ho et al., 2011), or to meet the standards required for discharge to sensitive water courses and drinking water protected areas (Defra, 2012).

Granular media filtration removes suspended solids and colloidal particles, which includes particulate biochemical oxygen demand (BOD), chemical oxygen demand (COD), microbes and other suspended chemical contaminants from wastewater secondary effluent (Illueca-Munoz et al., 2008). Removal of solids is also necessary prior to chemical and UV disinfection that may be used for wastewater reclamation (Lazarova et al., 1999; Williams et al., 2007) by reducing shielding of viruses by solid particles (Kirkpatrick et al., 1986). In the UK, tertiary filtration of wastewater secondary effluent is usually necessary in environmentally sensitive areas where tight regulatory discharge requirements are needed. Tertiary treatment is therefore becoming more common to safeguard public health as well as to minimise pollution (Ho et al, 2011; Langenbach et al., 2010; Li et al., 2012).

Filtration of wastewater is significantly more challenging than for potable water due to the higher solid loads, much of which is organic in nature. To illustrate, the average influent turbidity to a drinking water works filtration system is typically around 1 NTU with occasional spikes up to 8 NTU (Zouboulis et al., 2007). However, secondary effluents typically have turbidity between 5 to 20 NTU (TSS 10-40 mgL^{-1}) which causes rapid

headloss development in most conventional mono-media filters (Aronino et al., 2009; Lander, 1994). Aronino et al. (2009) observed cake formation on a single media depth filter treating wastewater secondary effluent and while the filter was effective for virus removal, the headloss build up was rapid. The increase in normalised headloss (NHL) per filtered volume was 1.65 $(m^3/m^{-2})^{-1}$ at a filtration rate of 5 mh^{-1}. Rapid headloss development shortens the filter runs and hence results in a low product water throughput before backwash is necessary.

One of the reasons for rapid headloss development in conventional mono-media filters is because the backwash cycle leads to media stratification, with small media grains at the top and large grains at the bottom (Baruth, 2005). The stratified arrangement leads to accumulation of the solids in the top layer in the subsequent filter cycle and hence results in underuse of the rest of the filter depth for solid retention. One proprietary mono-media filter (the Tetra filtration system) overcomes this through the use of coarse media of uniform size to discourage size stratification and also to promote deep penetration of solids (Crittenden et al., 2012). Use of coarse media, however, has a disadvantage in that it reduces surface area for particle capture. This may be overcome by operating the filter in an up-flow configuration, which has been shown to provide greater particle deposition (Chrysikopoulos and Syngouna, 2014). However, down-flow multimedia filters benefit from the use of both large and small media grains, using large grains of low density media and small grains of dense media. Such a design enables the backwash to stratify the filter bed keeping large grains at the top and small grains at the bottom; hence encouraging deep penetration of solids and improved removal performance with depth. This counters some of the operational problems associated with single media filters offering the opportunity for such filters to operate longer and at increased hydraulic loading therefore retaining more solids. In this research a quadruple media filter was studied consisting of layers of anthracite, flint, alumina and magnetite, moving from large to small grain size from top to bottom.

Previous studies involving granular media filters have investigated hydraulic loading rates (HLRs) up to 25 mh^{-1} (Williams et al., 2007; Li et al., 2012; Cleasby et al., 1962; Suthaker et al., 1995), rates typical of rapid gravity filters. Pressure filters have the capacity to operate at a higher rate (Tobiason et al., 2011). However, there is a paucity of information on particle capture when pressure filters operate at high HLRs. Operating the filter at higher rates is a cost effective means to increase throughput for the same area of filter bed. The aim of this research was to therefore investigate the effect of high hydraulic loading rate on the solids removal efficiency of a quadruple media filter treating wastewater secondary effluent. The contribution of each media layer was evaluated and the change in treated water particle size distribution (PSD) was assessed through each media layer.

Materials and Methods

Filtration tests

The investigation was carried out using a pilot plant located at a small sewage treatment works (STW) in the United Kingdom, filtering real secondary treated wastewater effluent. The STW treats 2,500 m^3d^{-1} of municipal wastewater using preliminary screening and grit removal, primary sedimentation, alum dosing, trickling filters and secondary sedimentation. Secondary effluent from the STWs discharge well was pumped to a mixed holding tank from where the feed was transferred to the filter rig (Figure 1). The quadruple media filter pilot plant was adapted using the same media layers as used in a commercial filter system (FilterClear, Bluewater Bio, UK). For the purpose of this study, the media were separated into different columns and connected in series so that the effect of each layer could be isolated. In the pilot plant, transfer between the layers had a retention time of less than 2 minutes, and particle size analysis confirmed that particle characteristics were not changed during transfer from one filter layer to the next. Wastewater was pumped from a holding tank

to the filter columns by a variable rate peristaltic pump (620 Industrial LoadSure, Watson Marlow, UK) through a flowmeter (SM6000, IMF Electronic Ltd, Germany). The filter rig consisted of four clear acrylic perspex columns of 700 mm height and 74 mm internal diameter. The columns were connected using PVC fittings and a clear PVC hose. Filter nozzles (Type KRI, KSHFisher, Germany) were fitted at the base of the columns to hold the filter media in place and evenly distribute the flow during the backwash cycle. The columns were connected so that the outlet of one column was fed into the inlet of the next.

Each column contained a different media at a depth of 100 mm. The media were anthracite (effective size, ES =1.12 mm, uniformity coefficient, UC =1.49, loose bed porosity, $\varepsilon_0 = 0.51$, sphericity, $\psi = 0.54$), flint (ES=0.55 mm, UC =1.42, $\varepsilon_0 = 0.52$, $\psi = 0.64$), alumina (ES=0.58 mm, UC =1.13, $\varepsilon_0 = 0.55$, $\psi = 0.63$) and magnetite (ES =0.26 mm, UC =1.54, $\varepsilon_0 = 0.47$, $\psi = 0.84$) respectively. A standard method was used to obtain the media effective size and uniformity coefficient (American Society for Testing and Materials (ASTM) C136-2006). The loose bed porosity ε_0 was determined by method ASTM C1252-2006 and the sphericity ψ was determined by calculations based on clean bed headloss measurement and the Kozeny-Carmen equation.

Online instruments for flow, pressure and turbidity were connected to the filter rig and the output analogue signals were logged into a laptop by an analogue-digital data logger (D-149, Dataq Instruments, UK). The columns were fitted with pressure transducers (PN2026, IMF Electronic Ltd, Germany) at the bottom and top of each media bed (100 mm apart) to measure the pressure drop across the filter bed. Sampling points were positioned at the influent and effluent to each column. The influent and effluent turbidity was monitored by probes placed in the influent holding tank and the effluent pipe (Turbi-Tech 2000LS and WaterWatch 2310, Partech, UK, respectively). The filter was run at a determined constant

flow rate (from 5 to 60 mh^{-1}) for each filter run and grab samples were collected on an hourly basis for analysis. Each flow rate condition was run in triplicate. At the end of the filter run, the columns were backwashed individually by an air scour (2 minutes) followed by high rate (60 mh^{-1}) water wash (10 minutes) using the filtrate. As each filter column could be isolated, it was not possible for the different media layers to mix with one another during filter backwash.

[FIG 1 HERE]

Performance Measurements

The total suspended solids (TSS) were determined from grab samples by gravimetric analysis Method 290D (APHA, 2005). Turbidity was measured in the laboratory using a turbidity meter (2100 Lab Turb, Hach, US). Zeta potential was measured by a zetasizer (Zetasizer Nano ZS, Malvern, UK). During sampling, the opening and closing of the sampling taps was carried out slowly to avoid hydraulic shocks in the system. The PSD of suspension particles was measured using a laser diffraction particle sizer (Spectrex PC-2200, Spectrex Corporation, California) within 30 minutes of sampling to minimize aggregation. The grab samples were diluted by a factor of 12 to reduce the effect of particle shielding at high concentrations.

Filtration models

Filtration was modelled using colloid filtration theory to show the effect of HLR on the retention of suspension particles by collectors, an approach used in drinking water filtration, but not to our knowledge in wastewater filtration. Filtration models have been defined assuming laminar flow conditions (Tobiason et al., 2011). To show that the filtration systems

used in this work was operating under laminar conditions, the Reynolds number was calculated from

$$\mathrm{Re}=\frac{\rho_w u d_{eq}}{\mu} \quad (1)$$

Where ρ_w is the water density, u is the superficial velocity, d_{eq} is the media equivalent diameter and μ is the dynamic viscosity. Re < 1 relates to Darcy flow, 1 < Re < 100 is Forchheimer flow, 600 < Re < 800 is transitional flow and 800 < Re is considered fully turbulent flow (Crittenden et al., 2012). In this study HLR of 5-60 mh^{-1} were investigated for which the Reynolds numbers for each media in the respective flow range were anthracite (2.2 < Re < 26.4), flint (0.9 < Re < 11.2), alumina (0.9 < Re < 11.4) and magnetite (0.6 < Re < 6.7). These Reynolds numbers were within the Darcy and Forchheimer flow regimes which are considered steady laminar flow and hence in the range where fundamental filtration models can be applied. These models, however, do not address the hydrodynamic variability in flow and the effect on streamlines introduced by the use of angular media (Crittenden et al., 2012). This was therefore an important element of investigation for this study.

HLR is a major factor affecting both particle deposition and detachment in filtration (Bai et al., 1997). The particle deposition rate was calculated from the single collector transport efficiency η and attachment efficiency α (Yao et al., 1971). The contact/transport efficiency is the rate at which approaching suspension particles contact the collector. This has been described analytically (Yao et al., 1971) and through regression analysis of numerical simulation data (Tufenkji et al., 2004; Rajagopalan and Tien, 1976) and takes into account the suspension hydrodynamics (Lander, 1994). The retention of particles (attachment efficiency) on collectors has mainly been explained in terms of the chemical interactions and adhesive forces such as the double layer forces and the London-van der Waals forces (Stumm

and Morgan, 1996; Tien, 2000), however the hydrodynamic conditions also have a strong influence on whether the particles are retained on collectors (Torkzaban et al., 2007). Adhesive forces depend on the physicochemical characteristics of the particles and media and are therefore independent of HLR. High HLR increases the hydrodynamic scouring force and can impair the retention of particles in the filter. The quadruple media filter has a tapered void; as such the channels between the collectors narrow down the bed, bringing particles nearer to the collectors hence increasing the chance of being captured. However hydrodynamic forces may also change in each media layer due to different bed porosities between layers. This investigation therefore explored the change in HLR and its direct influence on the hydrodynamic forces in each layer. The model demonstrated how hydrodynamic forces impact on the retention of particles on collectors and to demonstrate the change in suspension particle size changes through the media layers.

Hydrodynamic Forces

Particles near collectors are subject to hydrodynamic forces. Since the suspension particles are much smaller than the media grain, they can be modelled as small spheres on a collector plane (Bai et al., 1997). The hydrodynamic force acting on the particles can be resolved to two components, the hydrodynamic lifting force (F_l) (normal to the plane of the collector) and the hydrodynamic drag force (F_{Hydro}) (tangential to the collector) from Tien and Ramaroa (2007). The hydrodynamic lifting force is given by:

$$F_l = k_l d_p^3 (\mu\gamma)^{-0.5} \left(3\mu \frac{A_S}{d_m} \frac{u}{\varepsilon_0 - \sigma} \right)^{1.5} \quad (2)$$

Where k_l is the coefficient for lifting force, d_p is the suspended particle diameter, d_m is the filter media diameter, μ is the dynamic viscosity, ν is the kinematic viscosity, σ is the bulk specific deposit, ε_0 is the clean bed porosity, u is the filtration velocity and the porosity-

188 dependent parameter based on the Happel's flow model, A_S is defined as $2(1-p^5)/w$, and $w=2-3p+3p^5-2p^6$, $p= (1-\varepsilon)^{1/3}$. The lifting force acts in the same plane as the adhesion forces
190 between the particle and the media; it is assumed to be the force causing the particle to drift
191 away from the collector if it detaches (Tien and Ramaroa, 2007). The hydrodynamic drag
192 force on a particle is the component of the hydrodynamic force along the collector plane
193 given by:

$$F_{Hydro} = 2.551 \times 3\pi\mu \frac{A_S}{d_m} d_p^2 \frac{u}{\varepsilon_0 - \sigma} \quad (3)$$

194 The hydrodynamic drag force has an effect of either sliding or rolling the particle along the
195 collector depending on its point of action on the particle. This displacement is resisted by a
196 sliding frictional force (F_f) calculated as:

$$F_f = k_f \frac{6(1-\varepsilon_0)}{d_m} \frac{Hd_p}{12\delta^2} \quad (4)$$

197 Where k_f is the sliding friction coefficient, H is the Hamaker constant and δ is the particle-
198 media separation distance. The coefficient k_f may also be the rolling friction coefficient if the
199 mechanism of particle motion is rolling instead of sliding (Bergendahl and Grasso, 2003).
200 Both the hydrodynamic drag force and the sliding frictional force act tangentially to the
201 collector, such that the net tangential force (F_T) is given by $F_T = F_f - F_{Hydro}$. The
202 hydrodynamic drag force increases with filtration rate while the frictional force is
203 independent of the filtration rate.

204

205

206

Results and Discussion

Turbidity and TSS measurement

The wastewater influent to the filter had the following characteristics: TSS = 21±2 mgL^{-1}, turbidity = 10.2±0.9 NTU, temperature = 20±2 °C and pH = 7.6±0.3. The influent particles had a d(0.5) size of 20 μm. Wastewater TSS was linearly correlated to turbidity with a gradient of 2.3 $mgL^{-1}NTU^{-1}$ (root mean square fit of 0.7), this fits well with previously published data for secondary effluent having gradients of 2-2.4 $mgL^{-1}NTU^{-1}$ (Burton et al., 2003). The TSS removal versus turbidity removal efficiency correlates with a gradient of 0.78 (root mean square fit of 0.8). This comparison of removal efficiency shows that TSS removal efficiency was slightly less than turbidity removal efficiency since unlike turbidity, the TSS is insensitive to the contribution of very small particles that might pass through the filter paper. In this study turbidity was chosen over TSS measurement to evaluate the removal of suspended solids since turbidity can better detect small changes in solids concentration, particularly for the small particles in the system and because it was easier to obtain more data from online turbidity monitors. Williams et al. (2007) also found the removal of turbidity to be a representative measure of particle and bacteria removal and hence a good indicator of the overall filter performance.

Overall filter performance

Throughout the study, the influent wastewater turbidity was kept at 10.2±0.9 NTU. The average effluent turbidity increased from 1.9±0.1 NTU at 5.0 mh^{-1} to 6.8±0.5 NTU at 62.7 mh^{-1}; resulting in removals of 80 and 40% respectively for the quadruple filter (Figure a). The filter operated effectively throughout the duration of the experimental programme, with a stable effluent quality observed during each filter run of 8 hours. No inter-mixing of media was observed following backwashing, the media remained structurally stable and no

accumulation of solids or mud-balling was observed in the filters. The turbidity removal efficiency decreased almost linearly with increasing HLR. The turbidity removal results were compared with literature wastewater filtration removal for increasing HLR (2a). To facilitate comparison, the gradients of linear regression fits were used to demonstrate the change in turbidity removal per unit change in HLR (measured as $\%m^{-1}h$). For single media sand filters the suspended solid removal efficiency reduced by 4.4 $\%m^{-1}h$ for an initial influent turbidity of 35 NTU when the HLR changed from 5 to 10 mh^{-1} (Li et al., 2012). A separate study saw reductions of 3.9 $\%m^{-1}h$ for an initial turbidity of 10 NTU when the HLR increased from 5 to 15 mh^{-1} (Yu et al., 2015). In an anthracite-sand dual-media filter removal reduced by 1.25 $\%m^{-1}h$ for an initial turbidity of 6.5 NTU and the HLR increased from 12.2 to 24.4 mh^{-1} (Williams et al., 2007). In the present study, the quadruple-media filter had turbidity removal reducing by 0.67 $\%m^{-1}h$ for an initial influent turbidity of 10.2 NTU with HLR increasing from 5 to 60 mh^{-1}. Hence the increase in HLR has a greater impact on the filter removal efficiency for single media filters than for dual media filters. The impact was even less for the quadruple filter used here, demonstrating the smallest deterioration in effluent quality with increasing HLR was seen for the quadruple filter, even though the HLR was also over a much wider range. This comparison shows that increasing the number of filter layers buffers the effect of the increased HLR hence giving more robust filter performance.

In this study the removal efficiency of the top (anthracite) layer decreased quickly from 58 to 40% between 5 mh^{-1} and 10 mh^{-1}, a reduction of 3.5 $\%m^{-1}h$ (Figure 2c), a value similar to the literature values seen for a single media filter (4.4 $\%m^{-1}h$ in Li et al. (2012) and 3.9 $\%m^{-1}h$ in Yu et al. (2015)). The quicker change in removal efficiency across a single layer such as may be seen in conventional sand filters may be one of the key reasons why there has been reluctance to increase HLRs in conventional mono-media filters. There have been attempts to buffer the effect of increasing HLR on removal efficiency by increasing the coagulant dose or

changing the filter bed depth which works to some extent, but has the downside of quickly raising the filter headloss (Lawler and Nason, 2006). In this study, the impact became less abrupt for the combined anthracite and flint layers (2.1 $\%m^{-1}h$), for the combined anthracite, flint and alumina (1.7 $\%m^{-1}h$) and for the quadruple filter (1.2 $\%m^{-1}h$) in the HLR range 5 to 10 mh^{-1}, showing the moderation that the additional layers have when the HLR was increased (Figure 2c).

Increasing HLR was observed to significantly affect the particle sizes exiting the filter. Analysis of the 10^{th}, 50^{th} and 90^{th} percentile particle size showed that while influent particle size was consistent, the effluent particle sizes increased with the HLR (Figure b). This shows that retention of large particles became harder at high HLRs. Increasing the HLR also had the consequence of raising both the clean bed and filtration headloss due to increased frictional forces (Figure 2d). The NHL increase during a filter run was proportional to the mass deposition (specific deposit) and hence was a measure of mass retention (Mays et al., 2005). The NHL increase was calculated as $(\Delta H-\Delta H_0)/\Delta H_0$ where ΔH is the filtration headloss and ΔH_0 is the clean bed headloss. The increase in NHL rose with filtered volume at all HLRs (Figure 2d); however the rates of change (slopes of fitting lines) did not change significantly (0.0042-0.0164 $m^{-3}m^2$) compared to the large change in HLRs. This was because while high HLR leads to a high solids loading to the filter, the solids removal efficiency reduced at high flow rates (Figure 2a) such that fewer solids were retained per filtered volume. Therefore, the rate of increase in NHL remains low at high HLRs making filter operation possible under such conditions.

[FIG 2 HERE]

Individual filter layer performance

Each media layer contributed differently to the removal of solids. As wastewater particles penetrate down through the filter, the larger particles are removed and the overall solids concentration decreases. Therefore, the bottom filter layers receive particles that were not removed upstream or that have been detached from layers above. Solids removed by each layer also depended on the HLR. For example there was high removal efficiency for anthracite and flint (60% and 40% respectively) at flow rates of 5 mh^{-1} but much lower removal efficiencies of 10% at high HLRs of 60 mh^{-1} (Figure 3). Anthracite received a consistent turbidity influent at all different loading rates. The removal efficiency of the anthracite layer demonstrated the profile of a typical single media filter with increasing hydraulic loading (Figure 3a). Consequently the turbidity of the influent to the flint layer increased with HLR (Figure 3b). With the increasing turbidity load and HLR, the removal efficiency also decreased for the flint layer.

In contrast, the bottom two layers (alumina and magnetite) had removal efficiency which started at 15% at low flow rates increasing to a maximum of 20% at 25 mh^{-1} for alumina and 40 mh^{-1} for magnetite before dropping with a further increase in flow rate (Figure 3c and d). Although these media had comparatively lower solid removal efficiency, these layers receive much lower suspended solids loads that contained a large number of hard to remove small particles (Williams et al., 2007). The alumina and magnetite turbidity removal efficiency initially improved because of the increased quantity of solids reaching these layers as the HLR increased because of lower removal in upstream media layers. Raising the HLR transported solids deeper into the filter bed, however high HLR also increased hydrodynamic scouring which prevented further improvement in removal efficiency (discussed below).

[FIG 3 HERE]

The mass accumulation of solids in the filter per unit filter volume, termed specific deposit (Crittenden et al., 2012) was examined for each media at different HLRs. The suspended solids for specific deposit calculation was approximated by multiplying the turbidity measurements by the conversion factor of 2.3 $mgL^{-1}NTU^{-1}$ (from the regression line as discussed earlier). At low HLRs, most solids were retained on the anthracite layer (Figure 4). As the HLR increased, the specific deposit also increased due to the increased solid loading rate, but the continued rise was halted by the increased hydrodynamic scouring that limited the retention of solids. In anthracite and flint, the specific deposit rose up to a HLR of 25 mh^{-1} and then became constant with further increases in HLR (Figure 4a and b). In the alumina layer, the specific deposit increased to a maximum at 30 mh^{-1}, then dropped with increasing HLR (Figure 4c). The specific deposit in the magnetite layer continued to increase through the HLRs investigated, a feature that gives the filter added resilience (Figure 4d). As the HLR increased, the solids reaching downstream layers increased hence the improved solid retention of downstream layers.

For each filter run, increasing solid retention resulted in an increase in headloss through the filter bed (Veerapaneni and Weisner, 1997). The NHL change for the media layers of the quadruple media filter at different HLRs was quite different for each layer (Figure 4). The variation of HLR in this study was thought to affect the NHL change with solids retention in three main ways: (1) increased flow resistance due to increased friction at higher filtration velocity; (2) the differences in the compactness of solid deposits at different HLR (Veerapaneni and Weisner, 1997), and (3) the size of solids reaching each layer. For HLR up to 30 mh^{-1}, an increase in HLR was coupled by an increase in the flow resistance through the porous media hence an increase in the NHL was observed (Tien and Ramaroa, 2007).

Previous work has also shown that large particle deposits are more compact than deposits from small particles (Veerapaneni and Weisner, 1997). Here, the anthracite layer received large particles with a concurrent low increase in NHL, perhaps as a result of more compact deposits filling the large pores to a much lower degree than expected and hence providing less resistance to flow (Figure 4a). In comparison, the downstream layers had higher NHL increase since the the smaller pores received less compact particles that filled the pore space compartiavely more than for the upper layers. This effect was particularly noticeable at the low range of HLR (<15 mh^{-1}) investigated in this work (Figure 4b, c, d). For HLR of 40 mh^{-1} and above, a mich higher rate in NHL was expected than was observed (Figure 4). However, this was not seen in this work and may be explained by the differences in compactness of solid deposits with increasing HLR (Veerapaneni and Weisner, 1997). While there are differences in compactness of solids for different particle sizes, there are also differences in partcile compactness with increasng filrtration veolcity. Solids deposited at low HLR have a tendency to form more open deposits that occupy more pore space when compared to solids at high HLR (Veerapaneni and Weisner, 1997), hence there is a significant NHL increase for a relatively low specific deposit (Figure). At high HLR (>40 mh^{-1}), the NHL would be expected to increase. At high HLR, small solids formed compact deposits which occupied less pore space within the porous media hence moderating the headloss increase. For example, in the alumina layer, the NHL remained fairly stable while the specific deposit was rising with HLR in the alumina layer due to the solids being deposited compactly at high HLR (Figure 4c). Similar observations were seen in the anthracite, flint and magnetite layers at high HLR where the NHL did not increase appreciably.

The specific deposit and headloss development of the quadruple media filter occurred in all the media layers (Figure), therefore the entire depth of the filter was utilised for solids storage. High HLR was also seen to increase the deposition of solids in the downstream

353 layers as it caused solids to penetrate deeper into the bed (Kau and Lawler, 1995). The
354 utilization of the entire filter depth for solid storage ensured a slow overall headloss
355 development enabling the quadruple filter to be operated at high HLRs, a feature that would
356 not be operationally possible in single media filters.

357 [FIG 4 HERE]

358 ***Particle size analysis***

359 Further support for the changes in the removal efficiencies and headloss development
360 observed in this study were made by examining the changes in the PSDs with filter depth and
361 at different HLRs. The wastewater particle sizes decreased at each stage of the filter for all
362 HLRs; an example of the PSD through each filter layer has been shown for an HLR of 5 mh^{-1}
363 (Figure 5a). The influent PSD remained unchanged throughout all the filter runs while the
364 effluent sizes were observed to increase when the HLR rose (Figure b). Therefore when the
365 filter was run at higher HLRs, the particle sizes passing through the filter gradually increased,
366 for example, the median particle size d(50) in the filter effluent was 6.5 μm at 5 mh^{-1},
367 increasing to 15 μm at 60 mh^{-1} (Figure b).

368 One of the surprising observations seen in this work was the appearance of some large
369 particles in the filtered water. To demonstrate, the presence of 3 classes of particles in the
370 final filtered water that were >15 μm were seen (Figure 5c). As can be seen, there was a
371 significant increase in the presence of larger particles with increasing HLR. For example, at 5
372 mh^{-1}, more than 95% of solids >15 μm were removed, while at 60 mh^{-1}, this had reduced to
373 30% removal of solids that were between 15-30 mm and only 75% removal of solids between
374 50-100 μm.

To analyse the trend in turbidity and particle removal efficiency further, comparison was made to removal predicted from filtration models from Tufenkji and Elimelech (2004) (commonly called the TE model) (Figure d). The TE model parameters were assumed as: attachment efficiency $\alpha = 1$; suspension particle density $\rho_p = 1.05$ kgm^{-3}; $\rho_w = 998$ kgm^{-3} at temperature T = 20 ^{0}C; the Hamaker constant H = 10^{-20} J; and the transport efficiency η was calculated from media characteristics defined in the materials and methods section. Favourable attachment ($\alpha = 1$) was assumed for all particle sizes in the wastewater, following Tufenkji and Elimelech (2004). In the present research this was justified given the low magnitude of the charge on the wastewater particles (zeta potential between -10 and -12mV), indicative of particle destabilization. The TE model predicted near complete removal of particles >15 µm, while 10 µm particles were also very well removed across all HLRs (Figure d). Smaller particles were modelled to be progressively more poorly removed. For example at 20 mh^{-1}, 5 µm particles were removed by 50% while 1 µm particles were removed by only 28%. There was therefore a discrepancy in the predictions of the filtration model with the observed presence of larger particles in the filtrate, particularly with an increase in HLR above 20 mh^{-1}. It is proposed that the TE model overestimates the removal of large particles by not accounting for particle detachment that might occur as a result of hydrodynamic forces that become more and more relevant at high HLR (Crittenden et al., 2012). The effect of hydrodynamic forces on the retention of particles is explored further in the next section.

[FIG 5 HERE]

Impact of scouring on filter performance

Further understanding of the filter performance was achieved by analysing the hydrodynamic forces acting on particles in the filter bed as the HLR was changed. An increase in HLR intensified the hydrodynamic scouring on deposited solids with a consequence of reducing

399 particle retention (Tobiason et al., 2011). The modelled net tangential force for a clean bed (σ
400 = 0) for increasing particle size and HLR shows that large particles are subject to greater
401 hydrodynamic forces and the forces differ in each filter media layer (Figure a), a similar
402 observation to that made by Bai and Tien (1997). The effect of hydrodynamic force is
403 therefore likely to be much greater in wastewater filtration where there is usually a greater
404 proportion of large particles to be filtered than is the case in drinking water filtration.

405 The frictional force component (F_f) of the net tangential forces acting on a particle attached to
406 a collector does not vary with HLR, however the hydrodynamic drag force (F_{Hydro}) increases
407 with HLR. The net tangential force becomes negative when the hydrodynamic drag force
408 exceeds the frictional force with the implication that the particle is liable to slide along the
409 collector or get fragmented, hence increasing the chance of detachment. A particle detaches
410 from the collector when the net tangential force exceeds the attachment forces between the
411 particle and collector. The differences in the force balance for particles being removed by
412 different media demonstrates the spatial variation that may be experienced by particles
413 attached to media of different physical structure.

414 At low HLR, the net tangential force is positive for all particle sizes (Figure) such that scour
415 plays little to no role in removing particles from collectors hence the high removal efficiency.
416 As the HLR increases, the net tangential force on particles becomes more negative with the
417 effect being much greater on large particles compared to small ones (Bai and Tien, 1997).
418 This is therefore consistent with the observed increase in average particle sizes exiting each
419 media layer (Figure b) and also the rising influent turbidities to flint, alumina and magnetite
420 layers (Figure 3b, c, d) as it became difficult to retain particles at high HLRs. The changes in
421 net tangential force with HLR were also different for each media layer because of the
422 different bed properties (media size and shape and the bed porosity) and the range of particles

423 received by each media layer (Figure a). Although the surface plots illustrate the forces that
424 would be experienced by a range of particles (0-90 μm), the very negative net tangential
425 forces that might be experienced by larger particles (>50 μm) in the lower filter layers, would
426 not be seen in practice because the upper layers would have removed and retained these
427 particles (Figure a).

428 To investigate the effect of the net tangential force acting on particles in relation to the
429 particles observed to leave each filter layer in this study, the critical particle sizes reaching
430 each layer were examined. For the average influent particle size of 20 μm going on to the
431 anthracite layer, the scouring model predicts that these particles would be dislodged at an
432 HLR of 27 mh^{-1} (point A1 in Figure 6b). Observations were very close to this predicted
433 value, where the median particle size seen in the anthracite effluent was 15 μm (Figure b).
434 For 15 μm particles reaching the flint layer, the model predicted these particles would be
435 dislodged at 38 mh^{-1} (point A2 in Figure b), identical to what was observed at this HLR
436 (Figure b). Similarly, 12 μm particles reaching both alumina and magnetite would potentially
437 be dislodged at 57 mh^{-1} (point A3) and 38 mh^{-1} HLR respectively (Figure b). The observed
438 results agree very closely as the median particle size leaving the filter layers at both HLR
439 were approximately 12 μm in diameter (Figure b). The anthracite layer reached the critical
440 force first as it was the largest media and received the largest particles (Bai and Tien, 1997).
441 The removal efficiencies of alumina and magnetite were observed to drop for HLR beyond
442 40 mh^{-1} thus indicating a point where the buffering effect produced by the additional layers
443 began to fall (Figure c and d), a HLR similar to what the model predicted for flint and
444 magnetite. The specific deposit was also observed to drop after the critical HLR was reached
445 for each layer (Figure).

446 The hydrodynamic model was therefore successful in demonstrating the deviation between
447 the TE model and the observed results, the differences arising due to the scouring effect of
448 hydrodynamic forces at high HLRs. Wastewater has a significant amount of large particles
449 which are subject to larger detachment forces. The TE model does not account for
450 detachment of retained particles hence may therefore be more appropriate for modelling
451 drinking water filtration where the suspension particles are smaller and lower HLRs are
452 usually used.

453 [FIG 6 HERE]

454 **Conclusions**

455 The results from this work have shown that the impact of the increase in HLR for the
456 quadruple media filter was much less than for a single media filter as the system was buffered
457 by the additional layers moderating the loss of performance. High HLR transported solids
458 deeper into the filter bed hence the entire depth of the filter was used for solid storage,
459 ensuring the headloss was distributed to all media layers. The hydrodynamic model
460 successfully explained the observed solids removal and the PSD at changing HLR for the
461 quadruple filter treating wastewater secondary effluent. The hydrodynamic model also
462 explained the deviation of the TE Model from the observed results particularly at high HLR
463 by showing the effects of hydrodynamic scouring on particle retention. The implications of
464 this research are the possibilities of operating the quadruple media filter at high HLR (up to
465 40 mh^{-1}) to increase the throughput with a moderate impact on the effluent quality.

466

467

468

Acknowledgements

The authors greatly thank Dr Garry Hoyland, Richard Hartnett and Dr Caroline Huo at Bluewater Bio Ltd for funding and permitting the use of their patent technology to carry out this investigation.

Nomenclature		d(0.1)	10 percentile particle size
F_{Hydro}	hydrodynamic drag force	d(0.5)	50 percentile particle size
F_l	hydrodynamic lifting force	d(0.9)	90 percentile particle size
F_f	Frictional force	ε_0	clean bed porosity
k_l	Coefficient of lifting force	ε	filter bed porosity
k_f	Coefficient of sliding friction	p	$(1-\varepsilon)^{1/3}$
d_p	suspension particle diameter	w	$2-3p+3p^5-2p^6$
d_m	filter media diameter	A_s	$2(1-p^5)/w$
d_{eq}	Media equivalent diameter	ρ_w	Density of water
H	Hamaker constant	ψ	Filter media sphericity
ΔH	Headloss	μ	dynamic viscosity
ΔH_0	Clean bed headloss	δ	particle-media separation distance
u	filtration flow velocity	σ	bulk specific deposit
ES	Effective size	η	transport efficiency
UC	Uniformity Coefficient	α	attachment efficiency
HLR	Hydraulic loading rate	NHL	Normalized headloss

487

488

References

Burton, F. L.; Tchobanoglous, G.; Stensel, H. D. *Wastewater engineering: treatment and reuse*, 4th ed.; McGraw-Hill: Boston, 2003.

Han, S.; Fitzpatrick, C. S. B.; Wetherill, A. The impact of flow surges on rapid gravity filtration. *Water Res.* **2009**, *43* (5), 1171–1178.

Kim, J.; Lawler, D. F. The influence of hydraulic loads on depth filtration. *Water Res.* **2012**, *46* (2), 433–441.

Bloetscher, F.; Pleitez, F.; Hart, J.; Stambaugh, D.; Cooper, J.; Kennedy, K.; Sher Burack, L. Comparing Contaminant Removal Costs for Aquifer Recharge with Wastewater with Water Supply Benefits. *JAWRA J. Am. Water Resour. Assoc.* **2014**, *50* (2), 324–333.

Christou, A.; Eliadou, E.; Michael, C.; Hapeshi, E.; Fatta-Kassinos, D. Assessment of long-term wastewater irrigation impacts on the soil geochemical properties and the bioaccumulation of heavy metals to the agricultural products. *Environ. Monit. Assess.* **2014**, *186* (8), 4857–4870.

Chrysikopoulos, C.V.; Syngouna, V.I. Effect of gravity on colloid transport through water-saturated columns packed with glass beads: Modeling and experiments. *Environ. Sci. Technol.* **2014**, 48 (12), 6805-6813.

Ho, L.; Grasset, C.; Hoefel, D.; Dixon, M. B.; Leusch, F. D. L.; Newcombe, G.; Saint, C. P.; Brookes, J. D. Assessing granular media filtration for the removal of chemical contaminants from wastewater. *Water Res.* **2011**, *45* (11), 3461–3472.

Aronino, R.; Dlugy, C.; Arkhangelsky, E.; Shandalov, S.; Oron, G.; Brenner, A.; Gitis, V. Removal of viruses from surface water and secondary effluents by sand filtration. *Water Res.* **2009**, *43* (1), 87–96.

512 Defra. *Waste water treatment in the United Kingdom – 2012 Implementation of the European*
513 *Union Urban Waste Water Treatment Directive – 91/271/EEC*; London, 2012.

514 Illueca-Muñoz, J.; Mendoza-Roca, J. A.; Iborra-Clar, A.; Bes-Piá, A.; Fajardo-Montañana,
515 V.; Martínez-Francisco, F. J.; Bernácer-Bonora, I. wastewater reuse in europe.
516 *Desalination* **2008**, *222* (1-3), 222–229.

517 Lazarova, V.; Savoye, P.; Janex, M. L.; Blatchley, E. R.; Pommepuy, M. Advanced
518 wastewater disinfection technologies: State of the art and perspectives. In *Water*
519 *Science and Technology*; 1999; Vol. 40, pp 203–213.

520 Williams, G. J.; Sheikh, B.; Holden, R. B.; Kouretas, T. J.; Nelson, K. L. The impact of
521 increased loading rate on granular media, rapid depth filtration of wastewater. *Water*
522 *Res.* **2007**, *41* (19), 4535–4545.

523 Kirkpatrick, W. R.; Asano, T. Evaluation of Tertiary-Treatment Systems For Waste-Water
524 Reclamation and Reuse. *Water Sci. Technol.* **1986**, *18* (10), 83–95.

525 Langenbach, K.; Kuschk, P.; Horn, H.; Kästner, M. Modeling of slow sand filtration for
526 disinfection of secondary clarifier effluent. *Water Res.* **2010**, *44* (1), 159–166.

527 Li, Y.; Yu, J.; Liu, Z.; Ma, T. Estimation and modeling of direct rapid sand filtration for total
528 fecal coliform removal from secondary clarifier effluents. *Water Sci. Technol.* **2012**,
529 *65* (9), 1615–1623.

530 Zouboulis, a.; Traskas, G.; Samaras, P. Comparison of single and dual media filtration in a
531 full-scale drinking water treatment plant. *Desalination* **2007**, *213* (1-3), 334–342.

532 Lander, J. Wastewater rapid-gravity filtration in Severn Trent Water. *J. Inst. Water Environ.*
533 *Manag.* **1994**, *8* (3), 256–268.

534 Baruth, E. E. *Water treatment plant design*, 3rd ed.; McGraw-Hill: New York, 2005.

535 Crittenden, J. C.; Trussell, R. R.; Hand, D. W.; Howe, K. J.; Tchobanoglous, G. *Water*
536 *Treatment principle and design*; 2012.

537 Cleasby, J. L.; Baumann, E. R. Selection of Sand Filtration Rates. *J. Am. Water Works Assoc.*
538 **1962**, *54* (5), 579–602.

539 Suthaker, S.; Smith, D. W.; Stanley, S. J. Evaluation of Filter Media for Upgrading Existing
540 Filter Performance. *Environ. Technol.* **1995**, *16* (7), 625–643.

541 Tobiason, J.; Cleasby, J.; Logsdon, G.; O'Melia, C. Granular Media Filtration. In *Water*
542 *Quality & Treatment: A Handbook on Drinking Water*; Edzwald James, Ed.; American
543 Water Works Association, American Society of Civil Engineers, McGraw-Hill:
544 Massachusetts, 2011; p 10.1.

545 APHA, A.; and WEF. *Standard Methods for the Examination of Water and Wastewater*, 21st
546 ed.; Washington D.C., 2005.

547 Bai, R.; Tien, C. Particle Detachment in Deep Bed Filtration. *J. Colloid Interface Sci.* **1997**,
548 *186* (2), 307–317.

549 Yao, K.; Habibian, M. T.; O'Melia, C. R. Water and Waste Water Filtration: Concepts and
550 Applications. *Environ. Sci. Technol.* **1971**, *5* (11), 1105–1112.

551 Tufenkji, N.; Elimelech, M. Correlation Equation for Predicting Single-Collector Efficiency
552 in Physicochemical Filtration in Saturated Porous Media. *Environ. Sci. Technol.* **2004**,
553 *38* (2), 529–536.

554 Rajagopalan, R.; Tien, C. Trajectory analysis of deep-bed-filtration with the sphere-in-cell
555 porous media. *AIChE Journal*. 1976, pp 523–533.

556 Stumm, W.; Morgan, J. J. *Aquatic Chemistry: Chemical Equilibria and Rates in Natural*
557 *Waters*, 3rd ed.; John Wiley & Sons, Inc,: New York, 1996.

558 Tien, C. Hydrosol deposition in porous media: the effect of surface interactions. *Adv. Powder*
559 *Technol.* **2000**, *11* (1), 9–56.

560 Torkzaban, S.; Bradford, S. a.; Walker, S. L. Resolving the coupled effects of hydrodynamics
561 and DLVO forces on colloid attachment in porous media. *Langmuir* **2007**, *23* (19),
562 9652–9660.

563 Tien, C.; Ramarao, B. V. *Granular Filtration of Aerosols and Hydrosols*, 1st ed.; Elsevier
564 Ltd: Oxford, UK, 2007.

565 Bergendahl, J.; Grasso, D. Mechanistic basis for particle detachment from granular media.
566 *Environ. Sci. Technol.* **2003**, *37* (10), 2317–2322.

567 Yu, J.; Li, Y.; Liu, Z.; Zhang, W.; Wang, D. Impact of loading rate and filter height on the
568 retention factor in the model of total coliform (TC) removal in direct rapid sand
569 filtration. *Desalin. Water Treat.* **2015**, *54* (1), 140–146.

570 Lawler, D. F.; Nason, J. a. Granular media filtration: Old process, new thoughts. *Water Sci.*
571 *Technol.* **2006**, *53* (7), 1–7.

572 Mays, D. C.; Hunt, J. R. Hydrodynamic aspects of particle clogging in porous media.
573 *Environ. Sci. Technol.* **2005**, *39* (2), 577–584.

574 Veerapaneni, S.; Wiesner, M. R. Deposit Morphology and Head Loss Development in Porous
575 Media. *Environ. Sci. Technol.* **1997**, *31* (10), 2738–2744.

576 Kau, S. M.; Lawler, D. F. Dynamics of Deep-Bed Filtration : Velocity , Depth , and Media. *J.*
577 *Environ. Eng.* **1995**, *121* (1978), 850–859.

578

579

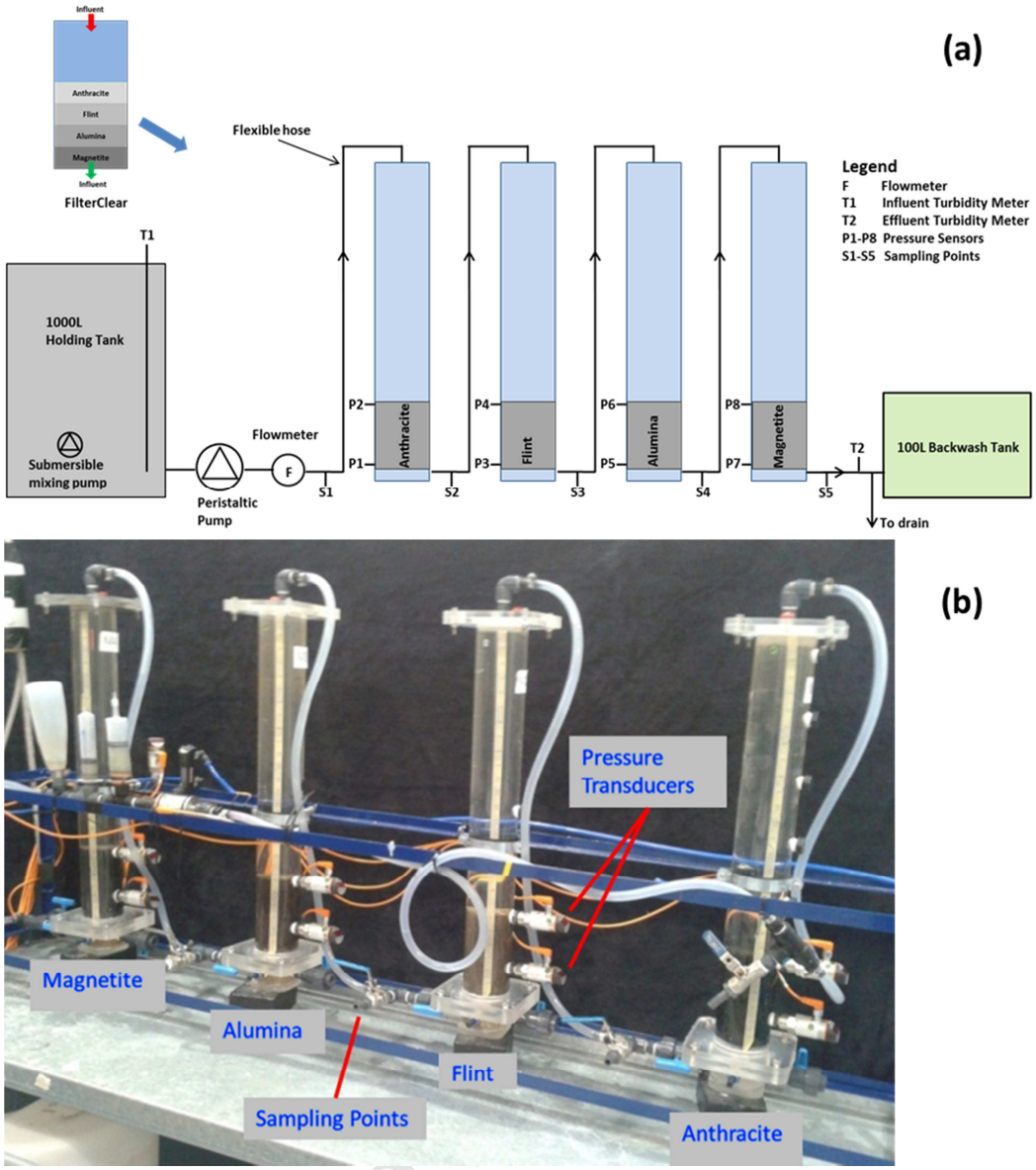

Figure 1: (a) Schematic and (b) photograph of the pilot filter rig.

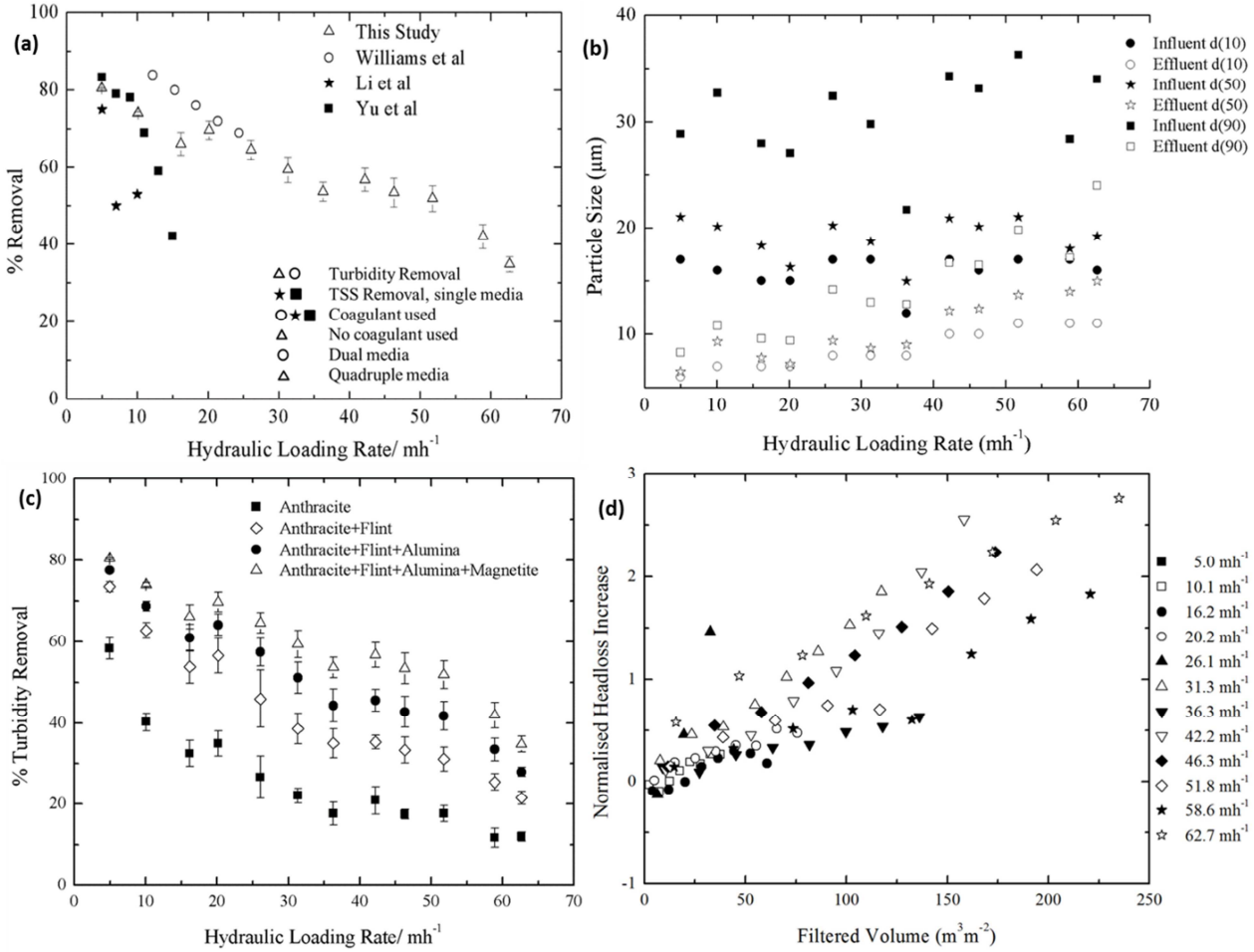

Figure 2: (a) Overall turbidity removal efficiency in this study and comparable data from previous studies, (b) d(10), d(50), d(90) particle sizes for both the influent and effluent at different HLRs. (c) The impact of HLR on the average filter turbidity removal efficiency for the quadruple (anthracite, flint, alumina and magnetite) filter, tri-media (anthracite, flint and alumina) filter, dual-media (anthracite and flint) filter and the mono-media (anthracite) filter, (d) Change in NHL increase with filtered volume at different HLRs.

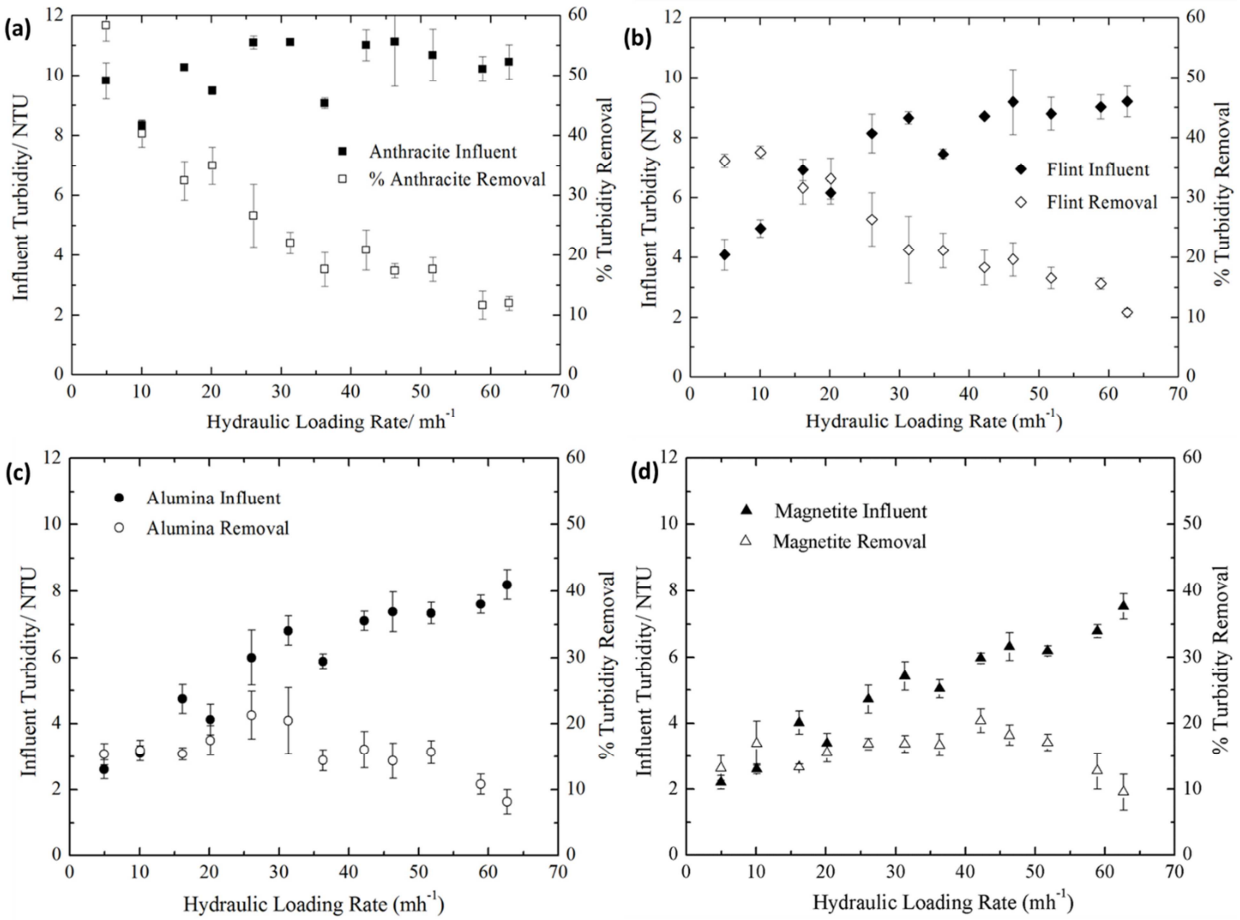

Figure 3: Turbidity removal for each media at different HLRs and the turbidity influent to each layer.

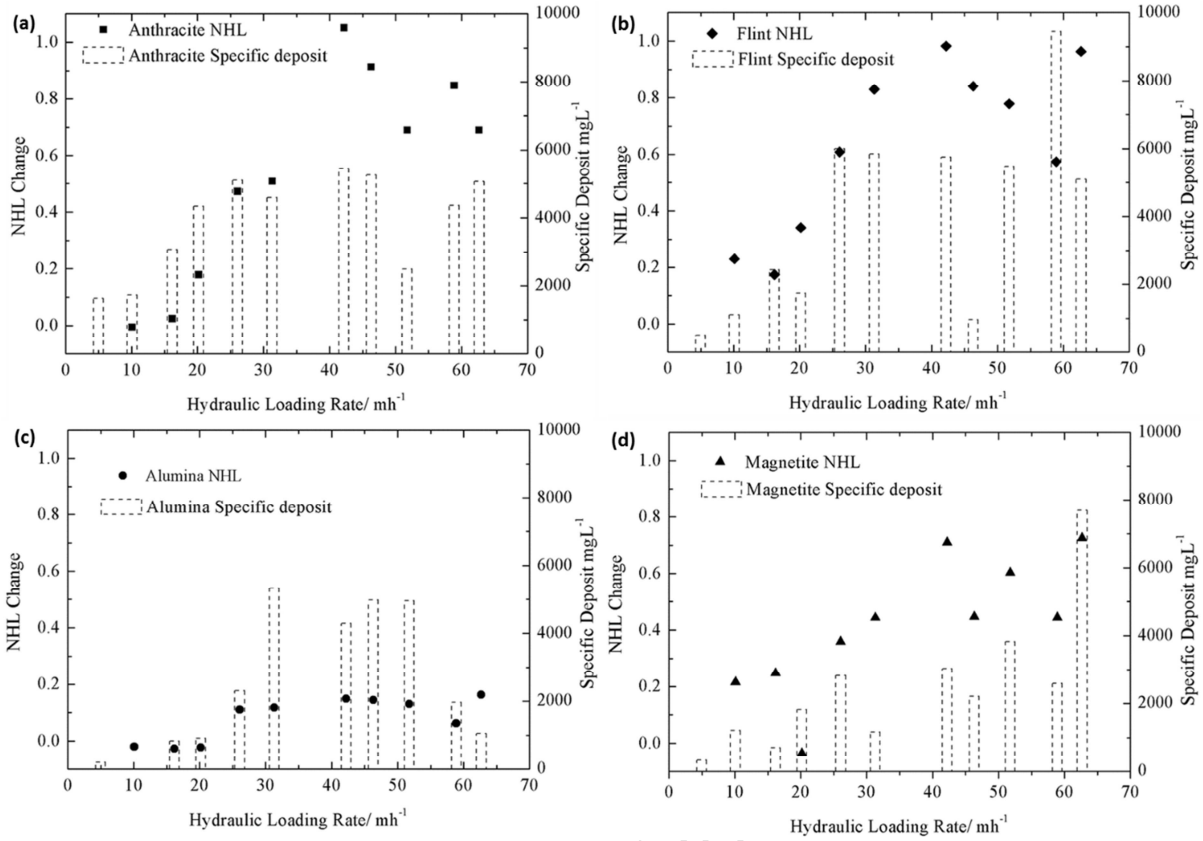

Figure 4: NHL change and specific deposit at different filtration rates for the four media.

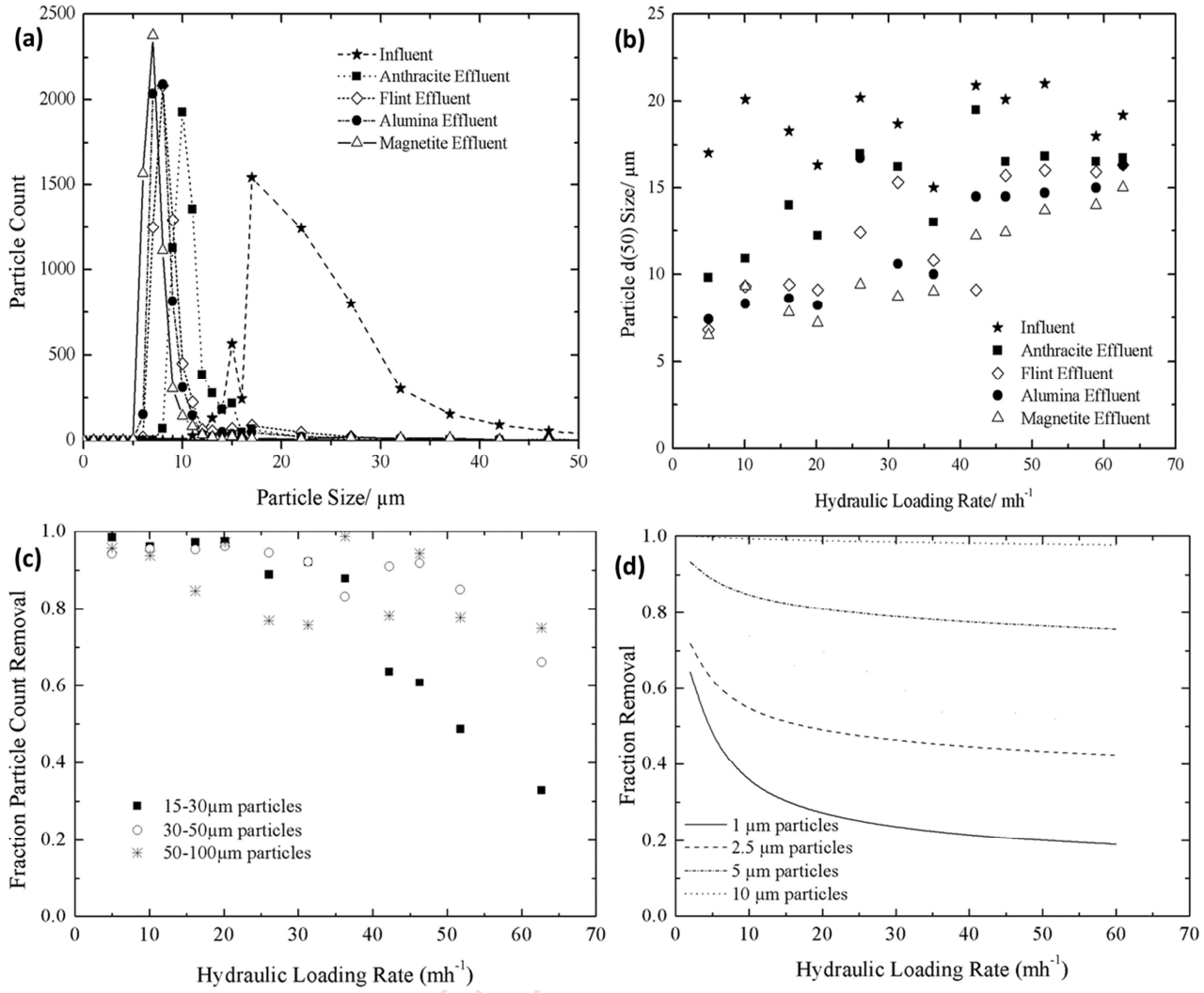

621

622 Figure 5: (a) Typical PSDs of the wastewater at different stages through the filter (for the 5
623 mh^{-1} filter run), (b) The average size of particles passing through each filter stage at different
624 HLRs, (c) Overall removal of 15-30 µm, 30-50 µm and 50-100 µm particles, (d) The TE
625 model plots for the particle sizes 1, 2.5, 5 and 10 µm.

626

627

628

629

630

631

632 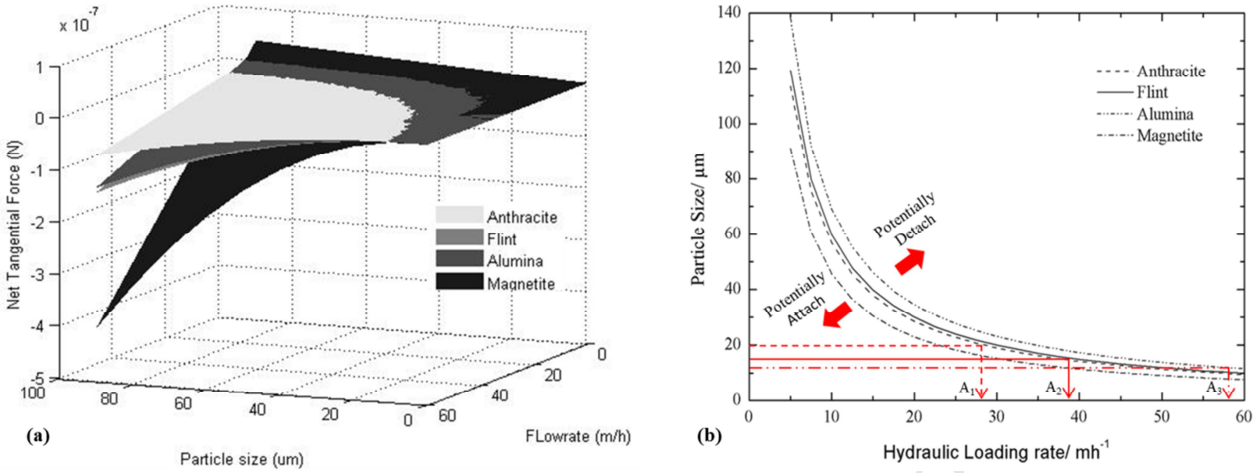

633 Figure 6: Modelled net tangential force (equation (3) and (4)) in a clean bed (σ = 0) (a) 3D
634 plot for the different particle sizes and HLRs in the four media layers, (b) Plot of the particle
635 sizes and HLR when the net tangential force is zero for the four layers ($k_f = 3.79\times10^{-6}$ m from
636 Bai and Tien (1997), H= 1.4×10^{-20} kgm^2s^{-2} and $\delta = 3\times10^{-10}$m [24], μ = 0.000955 $kgm^{-1}s^{-1}$ and
637 the parameters defined in Materials and Methods were used in the simulation).

638

Highlights

A multimedia filter successfully treated tertiary wastewater at rates up to 40 mh^{-1}

The impact of loading onto the multimedia filter was much less than for a single media filter

Hydrodynamic scouring models successfully explained the observed solids removal

The multimedia filter provides an effective way to provide enhanced wastewater treatment